• Basic Research •

Paeonol suppresses epithelial-mesenchymal transition-driven posterior capsular opacification through activation of AMPK signaling

Qing Wang[1,2], *Qing-Yu Li*[3,4], *Jing Yang*[2], *Jun Ma*[2], *Ji-Hua Ping*[2], *Zheng Wang*[5], *Dai-Jie Wang*[6], *Xia Hua*[7], *Xiao-Yong Yuan*[3,4]

[1]Clinical College of Ophthalmology, Tianjin Medical University, Tianjin 300070, China
[2]Department of Ophthalmology, Heze Medical College, Heze 274000, Shandong Province, China
[3]Department of Cataract, Tianjin Eye Hospital, Tianjin 300020, China
[4]Tianjin Key Lab of Ophthalmology and Visual Science, Tianjin 300020, China
[5]Department of Genetics and Cell Biology, Basic Medical College, Qingdao University, Qingdao 266071, Shandong Province, China
[6]International Joint Laboratory of Medicinal Food R&D and Health Products Creation/Biological Engineering Technology Innovation Center of Shandong Province, Heze Branch of Qilu University of Technology, Shandong Academy of Sciences, Heze 274000, Shandong Province, China
[7]Tianjin Aier Eye Hospital, Tianjin University, Tianjin 300040, China
Co-first Authors: Qing Wang and Qing-Yu Li
Correspondence to: Xia Hua. Tianjin Aier Eye Hospital, Tianjin University, Tianjin 300040, China. cathayhuaxia@163.com; Xiao-Yong Yuan. Department of Cataract, Tianjin Eye Hospital, Tianjin 300020, China. yuanxy_cn@hotmail.com
Received: 2025-09-08 Accepted: 2025-10-13

Abstract

● **AIM:** To determine whether paeonol (Pae), a naturally occurring phenolic compound, can serve as an effective pharmacological inhibitor of posterior capsular opacification (PCO).

● **METHODS:** A rat model of cataract surgery–induced PCO was established, and Pae was administered *via* anterior chamber injection to evaluate its preventive effect on capsular opacification and fibrotic remodeling. Histological and immunohistochemical analyses were performed to assess epithelial-mesenchymal transition (EMT)–related changes in lens epithelial cells (LECs). *Ex vivo* lens capsule cultures were employed to examine the expression of Vimentin and Zonula Occludens-1 (ZO-1) by immunofluorescence and immunohistochemistry. In the human LEC line SRA01/04, EMT marker expression at both mRNA and protein levels was analyzed following transforming growth factor beta 2 (TGF-β2) stimulation, with Pae treatment. Western blotting and immunofluorescence were used to investigate the effect of Pae on TGF-β/Smad signaling and AMP-activated protein kinase (AMPK) activation. Molecular docking was performed to predict Pae–AMPK binding, and rescue experiments with AMPK inhibition were conducted to validate the mechanistic pathway.

● **RESULTS:** Pae significantly reduced capsular opacification and fibrotic remodeling in the rat PCO model compared with controls. In LECs, Pae markedly suppressed TGF-β2–induced EMT, evidenced by decreased expression of mesenchymal markers, such as Vimentin, Fibronectin, Collagen 1A1, α-SMA and preserved epithelial junctional protein ZO-1. Mechanistically, Pae was predicted to directly interact with the catalytic pocket of AMPK, which was experimentally confirmed by enhanced AMPK phosphorylation and nuclear translocation (P<0.05). This activation disrupted canonical TGF-β/Smad signaling, leading to suppression of EMT. Rescue experiments using AMPK inhibition abrogated the anti-EMT effect of Pae, further validating the AMPK-dependent mechanism.

● **CONCLUSION:** Pae exerts a potent inhibitory effect on PCO formation by blocking EMT of LECs through direct activation of AMPK and subsequent disruption of TGF-β/Smad signaling.

● **KEYWORDS:** posterior capsular opacification; paeonol; epithelial-mesenchymal transition; AMP-activated protein kinase; transforming growth factor beta

DOI:10.18240/ijo.2026.02.02

Citation: Wang Q, Li QY, Yang J, Ma J, Ping JH, Wang Z, Wang DJ, Hua X, Yuan XY. Paeonol suppresses epithelial-mesenchymal transition-driven posterior capsular opacification through activation of AMPK signaling. *Int J Ophthalmol* 2026;19(2):219-229

INTRODUCTION

Posterior capsular opacification (PCO) is the most common long-term complication following cataract surgery and a leading cause of postoperative visual impairment[1-3]. PCO is primarily driven by residual lens epithelial cells (LECs) within the capsular bag[4-6]. Under altered aqueous humor conditions influenced by inflammation, oxidative stress, and surgical trauma, these cells undergo proliferation, migration, and epithelial-mesenchymal transition (EMT)[7-9]. EMT promotes excessive extracellular matrix deposition and capsular contraction, ultimately resulting in opacification and compromised visual function[10]. Although preventive strategies—such as optimized intraocular lens selection and refined surgical techniques—can reduce the incidence of PCO, they do not fully prevent its occurrence[11-12]. Epidemiological studies report an incidence of 11.8% within the first postoperative year, 20.7% within three years, and up to 28.4% within five years. The overall incidence ranges from 50% in adults within 2mo to 5y after surgery to nearly 100% in pediatric patients. Beyond visual deterioration, PCO interferes with posterior segment evaluation, including optical coherence tomography[1,13-14]. Neodymium: yttrium-aluminium-garnet (Nd:YAG) laser capsulotomy remains the standard intervention for clinically significant PCO, providing rapid visual restoration[15-16]. However, this procedure carries inherent risks, including intraocular lens damage, corneal endothelial loss, cystoid macular edema, and retinal detachment[17-19]. The residual surgical risk and potential irreversible complications underscore the need for safe and effective pharmacological approaches to prevent or mitigate PCO.

Paeonol (Pae) is a naturally occurring phenolic compound abundant in traditional medicinal plants, including the root of *Paeonia suffruticosa* and *Cortex moutan*[20]. It exhibits diverse pharmacological properties, such as antioxidant, anti-inflammatory, and antitumor activities[21-22]. Importantly, mechanistic studies have demonstrated that Pae can modulate EMT and fibrosis across multiple organ systems. For instance, Pae inhibits TGF-β1-induced EMT in pancreatic ductal adenocarcinoma cells by suppressing Smad 2/3 phosphorylation, thereby reducing cancer cell invasiveness and metastatic potential[23]. In models of hepatic fibrosis, Pae attenuates CCl_4-induced liver injury by inhibiting TGF-β1/Smad3 signaling and suppressing hepatic stellate cell activation[24]. Furthermore, Pae exhibits protective effects in cardiovascular and renal fibrotic models, mitigating extracellular matrix deposition, decreasing α-smooth muscle actin (α-SMA) expression, and restoring normal tissue architecture[25-27]. Despite these compelling findings, whether Pae can exert protective effects against ocular fibrotic disorders, particularly in PCO, remains unexplored.

Here, we demonstrate that Pae effectively prevents PCO using both *in vitro* human LEC models and *in vivo* rat models of capsular opacification. Pae directly engages AMP-activated protein kinase (AMPK), promoting its phosphorylation and nuclear translocation, which in turn inhibits canonical TGF-β/Smad signaling induced EMT, leading to reduced capsular opacification and fibrosis. These findings establish Pae as a promising pharmacological candidate for PCO prevention and highlight its potential as an alternative or adjunct to current surgical interventions.

MATERIALS AND METHODS

Ethical Approval All animal procedures were conducted in strict accordance with the ARVO Statement for the Use of Animals in Ophthalmic and Vision Research. The experimental protocol was approved by the Institutional Animal Care and Use Committee of Heze Medical College (Ethics Approval No.2025-007), ensuring compliance with established animal welfare standards.

Animals Sprague-Dawley rats (8-10 weeks old) were obtained from Jinan Jinfeng Laboratory Animal Co., Ltd. (Jinan, China) and housed under specific pathogen-free conditions at the Animal Research Center of Heze Medical College. Rats were randomly assigned to control and experimental groups.

Rat Model of Posterior Capsular Opacification SD rats were pretreated with 1% tropicamide in the right eye for 5min. General anesthesia was induced by intraperitoneal injection of propofol (100 mg/kg), supplemented with topical corneal anesthesia (proparacaine) and subconjunctival injection of lidocaine hydrochloride (0.1 mL). A corneal puncture was created approximately 2 mm from the limbus, followed by injection of viscoelastic into the anterior chamber. A 3-mm central anterior capsulotomy was performed using a custom-made needle, and hydrodissection was carried out to separate the lens capsule from the cortex. The corneal incision was then enlarged to 4–5 mm, and the lens nucleus was removed.

In the treatment group, the capsular bag and anterior chamber were filled with Pae (20 μmol/L; MCE, Shanghai, China) in balanced salt solution. In the control group, the capsular bag and anterior chamber were filled with balanced salt solution alone. The corneal incision was closed with 2–3 interrupted 10-0 nylon sutures, and 50 μL Pae solution (20 μmol/L) was reintroduced into the anterior chamber and capsular bag to maintain intraocular pressure within the physiological range.

Postoperatively, dexamethasone, gentamicin, and atropine were administered *via* peribulbar injection. Topical levofloxacin and pranoprofen were applied three times daily. The progression of PCO was assessed by slit-lamp biomicroscopy.

Lens Capsule Isolation and Culture Lens capsules were carefully dissected from SD rats under a stereomicroscope. Capsules were transferred immediately to M199 medium

(Gibco, Grand Island, NY, USA) and maintained under standard culture conditions. For experimental treatments, capsules were incubated with transforming growth factor beta 2 (TGF-β2; 10 ng/mL; R&D Systems Minneapolis MN, USA) and/or Pae (10 μmol/L).

Immunohistochemistry Rat eyes collected 60d post-surgery and lens capsules cultured for 7d were fixed in 4% paraformaldehyde (Beyotime, Shanghai, China) at 4°C for 12–16h, followed by standard paraffin embedding. Serial 4 μm sections were incubated with primary antibodies overnight at 4°C followed by incubation with corresponding secondary antibodies for 60min. Then sections were stained with diaminobenzidine tetrahydrochloride and counterstained with hematoxylin. A light microscope was used to generate images of immune stained samples. The following antibodies (dilution, manufacturer, location) were used in IHC experiments: Zonula Occludens-1 (ZO-1; 1:100; ABclonal, China) and Vimentin (1:100; HUABIO, China), HRP Goat anti-rabbit IgG (1:5000; ABclonal, China).

Cell Culture Human LECs (HLEC-SRA01/04, #CC4022, Guangzhou Saiku Biotech) were cultured in DMEM supplemented with 20% fetal bovine serum (FBS, Grand Island, NY, USA) under standard conditions (37°C, 5% CO_2, humidified). HLECs were divided into Control, TGF-β2 (10 ng/mL) groups, treated with or without Pae (10 μmol/L), or Compound C (1 μmol/L; MCE, Shanghai, China).

Immunofluorescence SRA01/04 cells were fixed in 4% paraformaldehyde for 15min, permeabilized with 0.5% Triton X-100 (Beyotime, Shanghai, China) for 20min, blocked with blocking buffer (Beyotime) for 2h at room temperature, and incubation with primary antibodies overnight at 4°C, and consequently incubated with secondary antibodies conjugated with fluorescein for 60min. Cell nuclei were counterstained with DAPI. Nikon ECLIPSE Ti confocal microscope (Nikon, Melville, NY, USA) was used to capture high-resolution images. The following antibodies (dilution, manufacturer, location) were used in IF experiments: Vimentin (1:100; HUABIO, China), ZO-1 (1:50; ABclonal, China), p-AMPK (1:100; Wanleibio, Shenyang, China), and p-Smad2/3 (1:50; Wanleibio, Shenyang, China).

Western Blotting Total protein from cells was extracted with RIPA buffer. Protein concentrations were measured by BCA Protein Assay Kit (Beyotime Biotechnology, Shanghai, China). The 40 μg of total protein were loaded and separated on SDS-PAGE gel, followed by transferred to PVDF membrane. The PVDF membrane was incubated with primary antibodies respectively after blocking in 5% skim milk in Tris-buffered saline with 0.1% Tween-20 (TBST). After washing with TBST 5min for three times, PVDF membranes were then incubated with secondary antibodies for 60min at room temperature. The signals were visualized with the ChemiDoc XRS+Imaging System (Bio-Rad Laboratories, Hercules, CA, USA). The bands density was quantified with Image Lab Software 6.0 (Bio-Rad Laboratories, software). All expression values were scaled to GAPDH. The following antibodies (dilution, manufacturer, location) were used in Western blots assay: Fibronectin (1:1000; HUABIO, China), ZO-1 (1:1000), Vimentin (1:2500), AMPK (1:250; ABclonal, China), p-AMPK (1:750), p-Smad2 (1:1000; HUABIO, China), p-Smad3 (1:1000; HUABIO, China), and Smad2/3 (1:1000; HUABIO, China).

RT-qPCR Total RNA was extracted using EZB-RN001-plus kit (EZBioscience, Roseville, MN, USA), and concentration/purity assessed with a Nanodrop 2000 spectrophotometer (Thermo Fisher). cDNA was synthesized from 1 μg RNA using Uni All-in-One Supermix (TransGen Biotech). Quantitative PCR was performed using SYBR Green (TransGen Biotech) to measure mRNA levels. All expression values were scaled to GAPDH. The sequences (from 5' to 3') of gene specific primers (forward primer; reverse primer) used in quantitative real-time RT PCR are: *COL1A1* (GAGGGCCAAGACGAAGACATC; CAGATCACGTCATCGCACAAC); *ACTA2* (TATC CCCGGGACTAAGACGG; CACCATCACCCCCTGATGTC); *FN'* (CGGTGGCTGTCAGTCAAAG; AAACCTCGGCTTCC TCCATAA); *TJP1* (ACCAGTAA GTCGTCCTGATCC; TCGGCCAAATCTTCTCACTCC); *VIM* (ATTCCACTT TGCGTTCAAGG; GCGAGAAATCC ACGTTCAAC); *GAPDH* (AATGGGCAGCCGTTAGGAAA; GCCCAATACGA CCAAATCAGAG).

Transwell Assay Cells were trypsinized, washed with PBS, and resuspended in serum-free medium. Transwell inserts (8 μm pore, 24-well) were seeded with 200 μL cell suspension (1×10^5 cells/mL), and 500 μL complete medium added to the lower chamber. After 7h, non-migrated cells were removed, and migrated cells were fixed with paraformaldehyde for 10min, stained with crystal violet for 30min, and imaged using a Leica DMi8 system.

Wound Healing Assay Confluent cells in 6-well plates were scratched with a 100 μL pipette tip. After washing, cells were incubated in medium containing TGF-β2, Pae, or Compound C. Images were acquired at 0, 12, and 24h, to monitor wound closure using a Leica DMi8 inverted microscope.

CCK-8 Assay Cells were seeded in 96-well plates at 4×10^4 cells/mL. After adherence, 10 μL CCK-8 reagent (Beyotime) was added per well and incubated for 24h. Optical density at 450 nm was measured using a BioTek plate reader.

Molecular Docking The crystal structure of AMPK (PDB ID: 5UFU) was retrieved from the Protein Data Bank. Ligand structures (Pae) were obtained from PubChem and prepared in SDF format. Protein structures were optimized by removing

water molecules, adding hydrogens, and energy minimization. The protonation state was set at pH 7. Active sites were identified using MOE 2008 alpha triangle method, and docking results were scored using London dG.

Statistical Analysis All experiments were repeated at least three times. Data are presented as mean±standard deviation (SD). Comparisons among multiple groups were performed using one-way ANOVA. Statistical analyses and figure generation were conducted with GraphPad Prism 9.0. $P<0.05$ was considered statistically significant.

RESULTS

Pae Inhibits Surgery- and TGF-β2-Induced Lens Capsule Fibrosis *in vivo* and *ex vivo* To determine whether Pae suppresses the development of PCO, we established a rat cataract surgery model and infused the anterior chamber with or without Pae. Over a 90-day follow-up, slit-lamp examination revealed that control eyes exhibited progressive PCO, characterized by capsular wrinkling and opacification. In contrast, Pae-treated eyes displayed markedly reduced capsular opacification at 30, 60, and 90d (Figure 1A). Histological analyses at day 60 further confirmed attenuated fibrotic remodeling in Pae-treated eyes, with reduced Vimentin expression and restoration of ZO-1 localization at the lens capsule (Figure 1B).

To complement these *in vivo* findings, *ex vivo* lens capsule explants were cultured under TGF-β2 stimulation. After 24h, immunofluorescence staining demonstrated robust induction of Vimentin in Control LECs, which was significantly suppressed by Pae treatment (Figure 1C). Notably, after 7d of culture, immunohistochemical analyses revealed pronounced LEC proliferation, migration, and Vimentin upregulation in TGF-β2-treated explants, accompanied by loss of ZO-1 (Figure 1D). Collectively, these data demonstrate that Pae attenuates both surgery- and TGF-β2-induced lens capsule fibrosis by maintaining the homeostasis of LEC.

Pae Suppresses TGF-β2-Induced EMT in HLECs It was well documented that EMT of HLECs drives key pathogenic processes underlying PCO. To determine whether Pae interferes with this response, we examined EMT induction in TGF-β2-treated HLECs. RT-qPCR analysis showed that TGF-β2 stimulation markedly upregulated EMT-associated genes, including COL1A1, fibronectin, Vimentin, and α-SMA, while suppressing the epithelial marker ZO-1. Pae treatment effectively reversed these transcriptional changes, restoring ZO-1 and attenuating mesenchymal gene expression. Notably, among the tested concentrations, 10 μmol/L Pae demonstrated the most potent inhibitory effect on TGF-β2–induced EMT, as evidenced by the most significant reversal of EMT-related gene expression (Figure 2A).

Functionally, Transwell and wound-healing assays revealed that Pae significantly reduced both vertical and horizontal migration of TGF-β2-treated HLECs. In wound-healing assays, Pae reduced horizontal migration by nearly 50% compared with TGF-β2-treated controls, while in Transwell assays, vertical migration was suppressed by approximately 40% (Figure 2B-2E). At the protein level, immunofluorescence demonstrated that Pae blocked TGF-β2-induced Vimentin upregulation and preserved ZO-1 expression (Figure 2F-2G). Western blot analysis confirmed these effects, showing decreased fibronectin and Vimentin levels and restored ZO-1 upon Pae treatment (Figure 2H-2I). Together, these findings establish that Pae effectively suppresses TGF-β2-induced EMT in HLECs, mitigating both molecular alterations and functional hallmarks of fibrotic transformation.

Pae Inhibits Smad Phosphorylation to Block TGF-β/Smad-Driven EMT Given that TGF-β is the principal inducer of EMT in HLECs, we next examined whether Pae modulates this process through the canonical TGF-β/Smad pathway. Immunofluorescence analysis showed that TGF-β2 stimulation triggered robust nuclear accumulation of phosphorylated Smad2/3, which was markedly suppressed by Pae treatment (Figure 3A). Consistently, Western blot analysis demonstrated that total Smad2/3 protein levels remained unchanged across conditions, whereas Pae significantly reduced TGF-β2-induced Smad2/3 phosphorylation (Figure 3B-3C). These data indicate that Pae modulate TGF-β2-mediated Smad signaling by preventing Smad2/3 phosphorylation and nuclear translocation, thereby blocking downstream EMT activation in HLECs.

Pae Activates AMPK Phosphorylation Through Direct Binding to AMPK To explore the direct target of Pae, we performed molecular docking, which showed strong binding affinity between Pae and AMPK (binding energy=-10.13 kcal/mol). Pae formed stable hydrogen bonds with ASP88 (2.76 Å) and LYS29 (2.38 Å), suggesting its potential to occupy the AMPK active pocket and promote phosphorylation (Figure 4A-4B). Supporting this prediction, Western blot analysis revealed that total AMPK protein levels remained unchanged across groups, whereas Pae markedly increased AMPK phosphorylation in TGF-β2–treated HLECs compared with TGF-β2 alone (Figure 4C-4D). Consistently, immunofluorescence staining confirmed enhanced p-AMPK expression in Pae-treated cells (Figure 4E). These findings indicate that Pae may directly activates AMPK phosphorylation in HLECs, providing a mechanistic basis for its antagonism of TGF-β/Smad-driven EMT.

AMPK Inhibition Abrogates the Anti-EMT Effects of Pae To further confirm AMPK activation is essential for Pae-mediated EMT inhibition, we used the selective AMPK inhibitor compound C. As expected, Pae treatment increased AMPK phosphorylation, accompanied by reduced Smad2

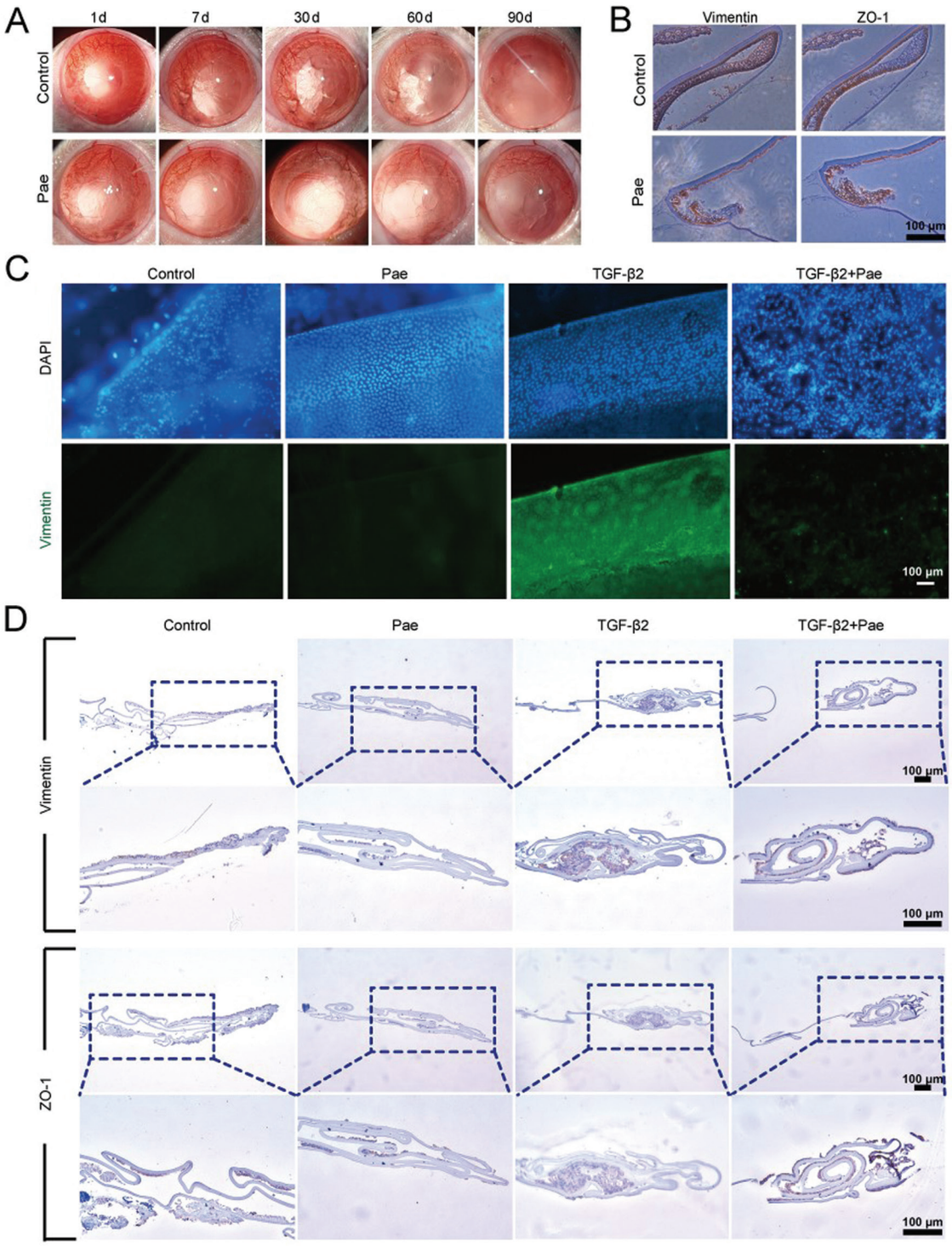

Figure 1 Pae suppresses TGF-β2-induced and surgery-induced lens capsule fibrosis in rats A: Slit-lamp microscopy of PCO development (1d, 7d, 30d, 60d, 90d) after extracapsular lens extraction, with or without Pae injected into the anterior chamber; B: Representative immunohistochemical images of lens capsule tissue from rat eyes 60d post-surgery (scale bar, 100 μm); C: Representative immunofluorescence staining of lens capsule explants for Vimentin in the presence or absence of Pae for 24h (scale bar, 100 μm); D: Representative immunohistochemical staining of rat lens capsule explants for Vimentin and ZO-1 treated with TGF-β2 in the presence or absence of Pae for 7d (scale bar, 100 μm). PCO: Posterior capsular opacification; Pae: Paeonol; ZO-1: Zonula Occludens-1; TGF-β2: Transforming growth factor beta 2.

and Smad3 phosphorylation. Co-treatment with compound C abolished these effects, restoring AMPK and Smad2/3 phosphorylation to levels similar to TGF-β2 treatment alone (Figure 5A-5D). In addition, Western blot analyses demonstrated that Pae suppressed mesenchymal gene expression (Vimentin) while restoring epithelial integrity marker ZO-1. Notably, these protective effects were reversed by compound C, which increased Vimentin expression and reduced ZO-1 to levels comparable to TGF-β2 treatment alone (Figure 5E-5F). Functional assays further supported

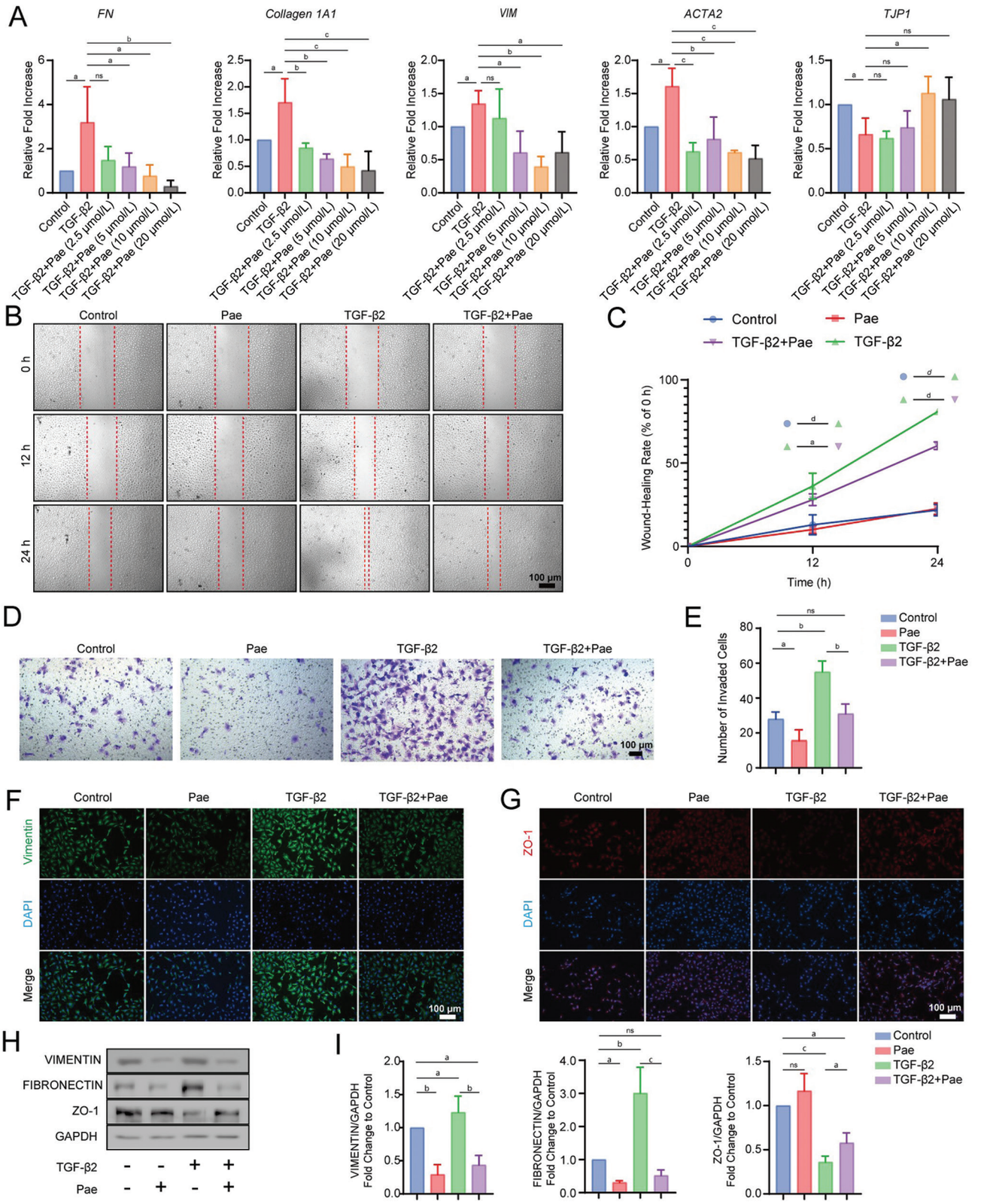

Figure 2 Pae inhibits TGF-β2-induced EMT in HLECs A: RT-qPCR analysis of EMT-related genes (COL1A1, FN, VIM, ACTA2, TJP-1) after 24h pre-treatment with or without Pae, followed by TGF-β2 stimulation for 24h (*n*=3); B: Wound-healing assay of HLECs treated with Pae; images captured at 0, 12, and 24h (scale bar, 100 μm); C: Quantification of wound-healing results; D: Transwell migration assay under the same conditions (scale bar, 100 μm); E: Quantification of the Transwell migration; F-G: Immunofluorescence staining of Vimentin (F) and ZO-1 (G) in treated HLECs; H: Western blot analysis of Vimentin, ZO-1, and fibronectin in treated HLECs; I: Quantification of Vimentin, ZO-1, and fibronectin proteins expression. Data are presented as mean±SD. One-way ANOVA: ns: $P>0.05$; $^{a}P<0.05$; $^{b}P<0.01$; $^{c}P<0.001$; $^{d}P<0.0001$. Pae: Paeonol; EMT: Epithelial-mesenchymal transition; HLECs: Human lens epithelial cells; TGF-β2: Transforming growth factor beta 2; ZO-1: Zonula Occludens-1; SD: Standard deviation.

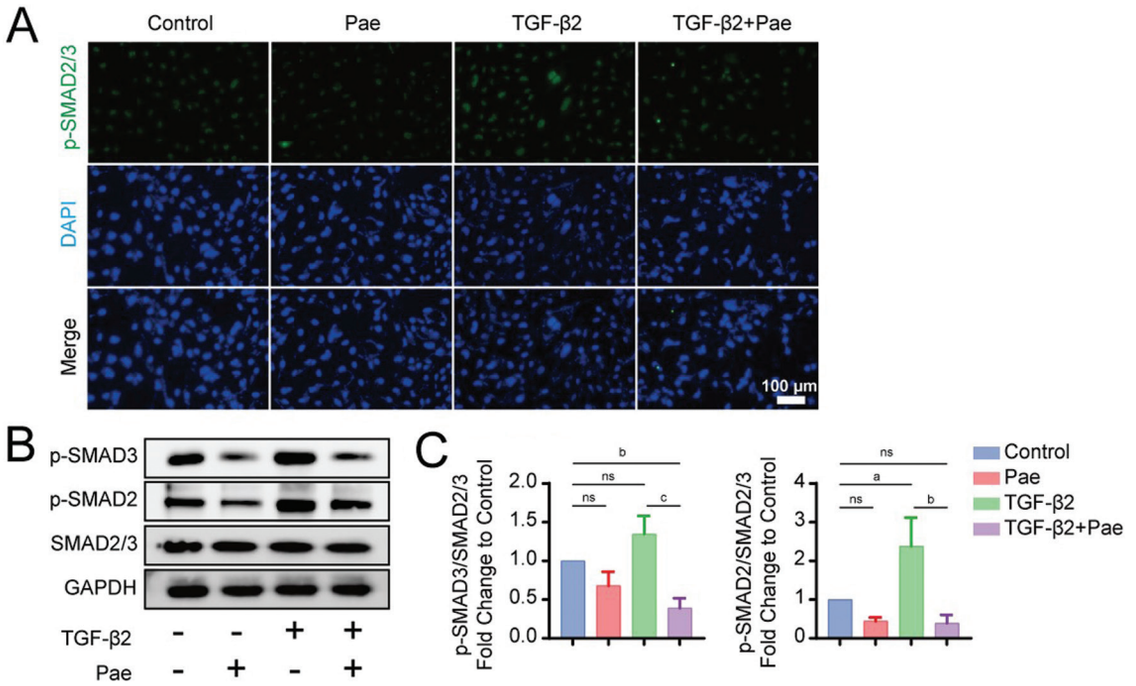

Figure 3 Pae inhibits Smad phosphorylation and blocks TGF-β/Smad-driven EMT in HLECs A: Immunofluorescence analysis of p-Smad2/3 in HLECs pre-treated with or without Pae for 24h, followed by TGF-β2 stimulation for 24h (scale bar, 100 μm; *n*=3); B: Western blot analysis of p-Smad2, p-Smad3, and total Smad2/3 under the same treatment conditions; C: Quantification of p-Smad2, p-Smad3, and total Smad2/3 proteins expression. Error bars indicate mean±SD. One-way ANOVA: ns: $P>0.05$; $^{a}P<0.05$; $^{b}P<0.01$; $^{c}P<0.001$. Pae: Paeonol; HLECs: Human lens epithelial cells; TGF-β2: Transforming growth factor beta 2; SD: Standard deviation.

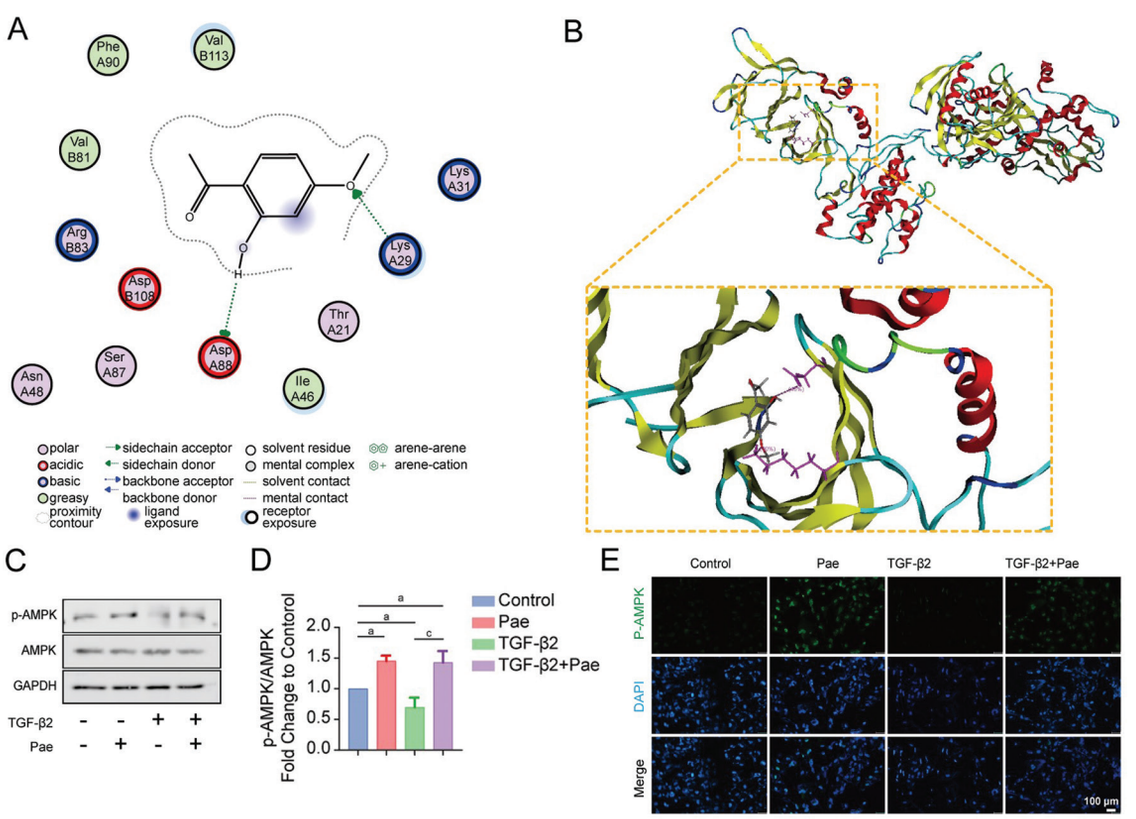

Figure 4 Pae activates AMPK phosphorylation *via* direct interaction with AMPK A: 2D representation of ligand–AMPK interactions showing hydrogen bonds between Pae and residues ASP88 and LYS29; B: 3D schematic of Pae binding within the AMPK active pocket; C: Western blot analysis of p-AMPK and total AMPK in HLECs pre-treated with or without Pae for 24h, followed by TGF-β2 stimulation for 24h; D: Quantification of p-AMPK and total AMPK proteins expression; E: Immunofluorescence staining showing enhanced p-AMPK expression in Pae-treated HLECs (scale bar, 100 μm). Error bars indicate mean±SD. One-way ANOVA: ns: $P>0.05$; $^{a}P<0.05$; $^{c}P<0.001$. Pae: Paeonol; HLECs: Human lens epithelial cells; TGF-β2: Transforming growth factor beta 2; AMPK: AMP-activated protein kinase; SD: Standard deviation.

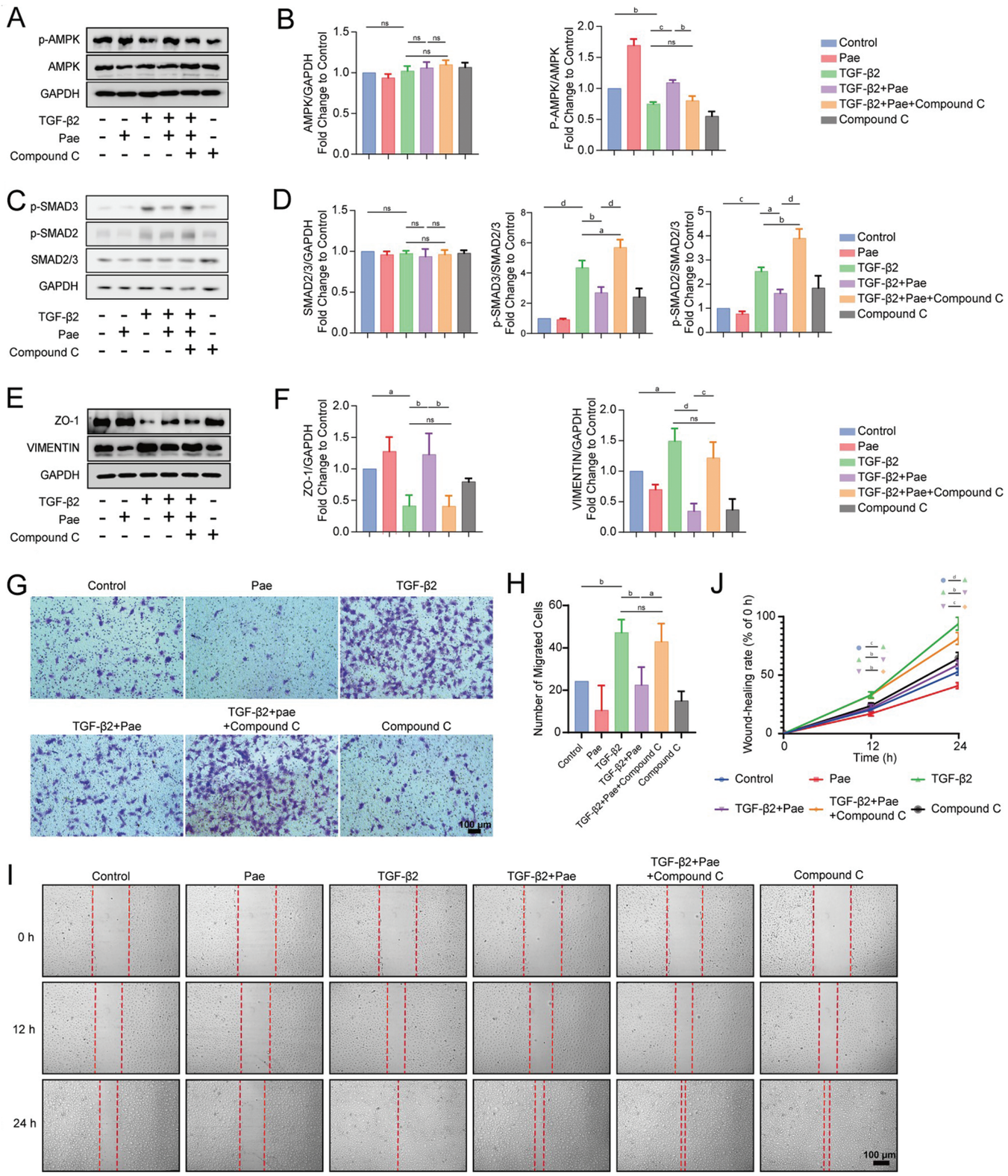

Figure 5 AMPK inhibition abrogates the anti-EMT effects of Pae in HLECs A: Western blot analysis of p-AMPK and total AMPK in HLECs pre-treated with or without Compound C, followed by Pae and/or TGF-β2 stimulation; B: Quantification of p-AMPK and total AMPK proteins expression; C: Western blot analysis of p-Smad2, p-Smad3, and total Smad2/3 in HLECs pre-treated with or without Compound C, followed by Pae and/or TGF-β2 stimulation; D: Quantification of p-Smad2, p-Smad3, and total Smad2/3 proteins expression; E: Western blot analysis of Vimentin and ZO-1 under the same conditions; F: Quantification of Vimentin and ZO-1 proteins expression; G: Transwell migration assay of treated HLECs (scale bar, 100 μm); H: Quantification of the Transwell migration; I: Wound-healing assay of treated HLECs; images captured at indicated time points (scale bar, 100 μm); J: Quantification of wound-healing results. Error bars indicate mean±SD. One-way ANOVA: ns: $P>0.05$; $^{a}P<0.05$; $^{b}P<0.01$; $^{c}P<0.001$; $^{d}P<0.0001$. Pae: Paeonol; EMT: Epithelial-mesenchymal transition; HLECs: Human lens epithelial cells; TGF-β2: Transforming growth factor beta 2; AMPK: AMP-activated protein kinase; ZO-1: Zonula occludens-1; SD: Standard deviation.

these findings. Both Transwell migration (Figure 5G-5H) and wound-healing assays (Figure 5I-5J) showed that Pae effectively suppressed vertical and horizontal migration of TGF-β2-treated HLECs. Strikingly, compound C significantly attenuated this inhibitory effect, restoring migratory capacity toward that of untreated controls. These data validate that AMPK activation as a critical upstream event required for Pae to suppress TGF-β2-induced EMT and migration in HLECs.

DISCUSSION

Current interventions to PCO, such as YAG laser posterior capsulotomy, which primarily achieve therapeutic effect by physically disrupting the posterior capsule. In this study, we identifies Pae as a pharmacological modulator of PCO through direct targeting of the AMPK/Smad signaling axis[28-30]. Pae acts upstream of fibrotic signaling, preventing LEC, EMT and fibrotic remodeling at the molecular level.

TGF-β/Smad signaling is the central driver of EMT in PCO. Consistent with this paradigm, TGF-β2 stimulation robustly induced EMT in human LECs, as evidenced by increased expression of mesenchymal markers, including Vimentin and fibronectin, along with suppression of epithelial markers such as ZO-1[31-32]. Pae treatment effectively reversed these molecular changes and suppressed functional hallmarks of EMT, including both horizontal and vertical cell migration[23]. These findings demonstrate that Pae interferes with TGF-β2-driven fibrotic signaling and preserves epithelial integrity in LECs, providing a pharmacological complement to surgical prevention strategies.

Mechanistically, our data indicate that Pae directly interacts with AMPK at its catalytic pocket, forming stable hydrogen bonds with key residues ASP88 and LYS29, thereby stabilizing AMPK in an active conformation and promoting its phosphorylation. Importantly, biochemical analyses confirmed that Pae enhanced AMPK phosphorylation without altering total AMPK protein levels, indicating that it functions as a natural AMPK activator. This mode of regulation differs from classical pharmacological AMPK agonists and highlights a novel mechanism linking energy sensing to fibrotic control[33]. Previous studies have shown that AMPK activation attenuates fibrosis in multiple organs, including liver[34], kidney[35-36], lung[37-38], and heart[39], primarily through inhibition of TGF-β-driven transcription and extracellular matrix deposition[40]. Our findings extend this paradigm to ocular fibrosis, demonstrating that AMPK activation can suppress Smad-dependent transcription and EMT in LECs, thereby connecting systemic anti-fibrotic pathways to local ocular pathology.

The functional relevance of AMPK activation was further validated using the selective inhibitor Compound C[41-42]. Pre-treatment with Compound C abolished Pae-induced AMPK phosphorylation, reversed suppression of EMT markers, and restored HLEC migration. These results establish AMPK as the critical upstream mediator of Pae's anti-EMT effects, suggesting a hierarchical interplay between metabolic sensing and TGF-β/Smad signaling in fibrotic progression. AMPK acts as a negative regulator of Smad-dependent transcription, providing direct evidence for its therapeutic potential in ocular fibrosis and filling a gap in pharmacological strategies for PCO prevention. While our mechanistic studies were performed *in vitro*, confirming AMPK activation in the rat PCO model would provide important *in vivo* evidence. This represents a limitation of the current work and a priority for future investigation.

Previous studies have shown that Pae inhibits TGF-β1-induced EMT in pancreatic cancer cells[23], attenuates hepatic fibrosis by suppressing hepatic stellate cell activation, and reduces extracellular matrix deposition in cardiovascular and renal fibrosis[26-27,43-44]. Our study extends these observations to ocular fibrosis, demonstrating for the first time that Pae suppresses TGF-β2-induced EMT in HLECs and attenuates post-surgical capsular fibrosis *in vivo*. Notably, the effect of Pae on AMPK activation provides a new mechanistic insight, complementing prior reports focusing on its antioxidant and anti-inflammatory activities. By directly engaging AMPK and indirectly inhibiting Smad2/3 phosphorylation, Pae bridges metabolic sensing and fibrotic signaling in LECs, underscoring its potential as a targeted pharmacological agent for PCO prevention.

From a translational perspective, the natural origin and favorable safety profile of Pae make it a promising candidate for intraocular application[45]. Compared with synthetic AMPK agonists, Pae may offer a safer and more biocompatible option for prophylactic treatment following cataract surgery. Its ability to modulate multiple pathogenic pathways—including EMT, oxidative stress, and inflammation—suggests that Pae may provide broad-spectrum protection against fibrotic eye diseases beyond PCO. Future directions include optimizing drug delivery systems, such as nanoparticle formulations or sustained intraocular delivery platforms, to achieve prolonged therapeutic activity, as well as exploring combinatorial strategies with current surgical or pharmacological interventions[46].

In summary, our findings identify Pae as a natural AMPK activator that disrupts TGF-β/Smad signaling and suppresses EMT-driven fibrosis in the lens capsule. By linking metabolic sensing to fibrotic regulation, Pae establishes a mechanistic foundation for pharmacological PCO prevention and highlights a broader potential for AMPK-targeted therapies in ocular fibrosis.

ACKNOWLEDGEMENTS

Authors' Contributions: Yuan XY conceived and designed the study. Wang Q, Yang J, and Ma J performed the

experiments. Ping JH and Li QY performed the analyses. Wang Q and Li QY wrote the paper. Wang Z and Wang DJ edited the manuscript. Hua X and Yuan XY reviewed the manuscript. All the authors read and approved the final submitted manuscript.

Data Availability: Data sharing is not applicable to this article as no new data were created or analyzed in this study.

Foundations: Supported by the Projects of Medical and Health Technology Development Program in Shandong Province (No.202107021009); Shandong Provincial Traditional Chinese Medicine Science and Technology Project (No.M-2023118).

Conflicts of Interest: Wang Q, None; **Li QY,** None; **Yang J,** None; **Ma J,** None; **Ping JH,** None; **Wang Z,** None; **Wang DJ,** None; **Hua X,** None; **Yuan XY,** None.

REFERENCES

1 Konopińska J, Młynarczyk M, Dmuchowska DA, *et al*. Posterior capsule opacification: a review of experimental studies. *J Clin Med* 2021;10(13):2847.

2 Nibourg LM, Gelens E, Kuijer R, *et al*. Prevention of posterior capsular opacification. *Exp Eye Res* 2015;136:100-115.

3 Lu CZ, Yu SS, Song H, *et al*. Posterior capsular opacification comparison between morphology and objective visual function. *BMC Ophthalmol* 2019;19(1):40.

4 Jiang J, Shihan MH, Wang Y, *et al*. Lens epithelial cells initiate an inflammatory response following cataract surgery. *Invest Ophthalmol Vis Sci* 2018;59(12):4986-4997.

5 Shihan MH, Novo SG, Duncan MK. Cataract surgeon viewpoints on the need for novel preventative anti-inflammatory and anti-posterior capsular opacification therapies. *Curr Med Res Opin* 2019;35(11): 1971-1981.

6 Sachdev GS, Soundarya B, Ramamurthy S, *et al*. Impact of anterior capsular polishing on capsule opacification rate in eyes undergoing femtosecond laser-assisted cataract surgery. *Indian J Ophthalmol* 2020;68(5):780-785.

7 Nishi O, Nishi K, Ohmoto Y. Synthesis of interleukin-1, interleukin-6, and basic fibroblast growth factor by human cataract lens epithelial cells. *J Cataract Refract Surg* 1996;22(Suppl 1):852-858.

8 Wei ZB, Caty J, Whitson J, *et al*. Reduced glutathione level promotes epithelial-mesenchymal transition in lens epithelial cells *via* a Wnt/β-catenin-mediated pathway: relevance for cataract therapy. *Am J Pathol* 2017;187(11):2399-2412.

9 Li CS, Yan WJ, Yan H. Oxidative stress, glutaredoxins, and their therapeutic potential in posterior capsular opacification. *Antioxidants* (*Basel*) 2024;13(10):1210.

10 Ma JY, Sun QH, Chen YJ, *et al*. Exosomes containing miR-148a-3p derived from mesenchymal stem cells suppress epithelial-mesenchymal transition in lens epithelial cells. *Stem Cells Transl Med* 2025;14(2):szae091.

11 Maedel S, Evans JR, Harrer-Seely A, *et al*. Intraocular lens optic edge design for the prevention of posterior capsule opacification after cataract surgery. *Cochrane Database Syst Rev* 2021;8(8):CD012516.

12 Belda JI, Dabán JP, Elvira JC, *et al*. Nd: YAG capsulotomy incidence associated with five different single-piece monofocal intraocular lenses: a 3-year Spanish real-world evidence study of 8293 eyes. *Eye (Lond)* 2022;36(11):2205-2210.

13 Wei ZB, Gordon P, Hao CL, *et al*. Aged lens epithelial cells suppress proliferation and epithelial-mesenchymal transition-relevance for posterior capsule opacification. *Cells* 2022;11(13):2001.

14 Shen HQ, Zhang H, Gong W, *et al*. Prevalence, causes, and factors associated with visual impairment in a Chinese elderly population: the Rugao longevity and aging study. *Clin Interv Aging* 2021;16:985-996.

15 Ling R, Borkenstein EM, Borkenstein AF. Evaluation of Nd: YAG laser capsulotomy rates in a real-life population. *Clin Ophthalmol* 2020;14:3249-3257.

16 Bhargava R, Kumar P, Sharma SK, *et al*. A randomized controlled trial of peeling and aspiration of Elschnig pearls and neodymium: yttrium-aluminium-garnet laser capsulotomy. *Int J Ophthalmol* 2015;8(3): 590-596.

17 Borkenstein AF, Borkenstein EM. Neodymium-doped yttrium aluminum garnet (Nd:YAG) laser treatment in ophthalmology: a review of the most common procedures Capsulotomy and Iridotomy. *Lasers Med Sci* 2024;39(1):167.

18 Hu CY, Woung LC, Wang MC, *et al*. Influence of laser posterior capsulotomy on anterior chamber depth, refraction, and intraocular pressure. *J Cataract Refract Surg* 2000;26(8):1183-1189.

19 Karahan E, Tuncer I, Zengin MO. The effect of Nd:YAG laser posterior capsulotomy size on refraction, intraocular pressure, and macular thickness. *J Ophthalmol* 2014;2014:846385.

20 Gong XB, Yang Y, Huang LG, *et al*. Antioxidation, anti-inflammation and anti-apoptosis by paeonol in LPS/d-GalN-induced acute liver failure in mice. *Int Immunopharmacol* 2017;46:124-132.

21 Zhang L, Li DC, Liu LF. Paeonol: pharmacological effects and mechanisms of action. *Int Immunopharmacol* 2019;72:413-421.

22 Latif S, Choi SH, Gyawali A, *et al*. Antioxidant and neuroprotective effects of paeonol against oxidative stress and altered carrier-mediated transport system on NSC-34 cell lines. *Antioxidants (Basel)* 2022;11(7):1392.

23 Cheng CS, Chen J-X, Tang J, *et al*. Paeonol inhibits pancreatic cancer cell migration and invasion through the inhibition of TGF-β1/smad signaling and epithelial-mesenchymal-transition. *Cancer Manag Res* 2020;12:641-651.

24 Wu SW, Liu LC, Yang S, *et al*. Paeonol alleviates CCl_4-induced liver fibrosis through suppression of hepatic stellate cells activation *via* inhibiting the TGF-β/Smad3 signaling. *Immunopharmacol Immunotoxicol* 2019;41(3):438-445.

25 Wu M, Yu ZL, Li XY, *et al*. Paeonol for the treatment of atherosclerotic cardiovascular disease: a pharmacological and mechanistic overview. *Front Cardiovasc Med* 2021;8:690116.

26 Zhang L, Chen ZQ, Gong WY, *et al*. Paeonol ameliorates diabetic renal fibrosis through promoting the activation of the Nrf2/ARE pathway *via* up-regulating Sirt1. *Front Pharmacol* 2018;9:512.

27 Zhou H, Qiu ZZ, Yu ZH, *et al*. Paeonol reverses promoting effect of the HOTAIR/miR-124/Notch1 axis on renal interstitial fibrosis in a rat model. *J Cell Physiol* 2019;234(8):14351-14363.

28 Gonzalez DM, Medici D. Signaling mechanisms of the epithelial-mesenchymal transition. *Sci Signal* 2014;7(344):re8.

29 Chen XY, Ye SB, Xiao W, *et al*. ERK1/2 pathway mediates epithelial-mesenchymal transition by cross-interacting with TGFβ/Smad and Jagged/Notch signaling pathways in lens epithelial cells. *Int J Mol Med* 2014;33(6):1664-1670.

30 Liu HF, Jiang B. Let-7a-5p represses proliferation, migration, invasion and epithelial-mesenchymal transition by targeting Smad2 in TGF-b2-induced human lens epithelial cells. *J Biosci* 2020;45:59.

31 Chen X, Yan H, Chen Y, *et al*. Moderate oxidative stress promotes epithelial-mesenchymal transition in the lens epithelial cells *via* the TGF-β/Smad and Wnt/β-catenin pathways. *Mol Cell Biochem* 2021;476(3):1631-1642.

32 Li H, Yuan XY, Li J, *et al*. Implication of Smad2 and Smad3 in transforming growth factor-β-induced posterior capsular opacification of human lens epithelial cells. *Curr Eye Res* 2015;40(4):386-397.

33 Dandapani M, Hardie DG. AMPK: opposing the metabolic changes in both tumour cells and inflammatory cells. *Biochem Soc Trans* 2013;41(2):687-693.

34 Jurado-Aguilar J, Barroso E, Bernard M, *et al*. GDF15 activates AMPK and inhibits gluconeogenesis and fibrosis in the liver by attenuating the TGF-β1/SMAD3 pathway. *Metabolism* 2024;152:155772.

35 Han S, Choi H, Park H, *et al*. Omega-3 fatty acids attenuate renal fibrosis *via* AMPK-mediated autophagy flux activation. *Biomedicines* 2023;11(9):2553.

36 Lu JM, Shi JH, Li MX, *et al*. Activation of AMPK by metformin inhibits TGF-β-induced collagen production in mouse renal fibroblasts. *Life Sci* 2015;127:59-65.

37 Cheng DM, Xu Q, Wang Y, *et al*. Metformin attenuates silica-induced pulmonary fibrosis *via* AMPK signaling. *J Transl Med* 2021;19(1):349.

38 Yu JW, Lu WH. Melittin alleviates bleomycin-induced pulmonary fibrosis *in vivo* through regulating TGF-β1/Smad2/3 and AMPK/SIRT1/PGC-1α signaling pathways. *Iran J Basic Med Sci* 2025;28(4):426-433.

39 Zhang J, Huang LL, Shi X, *et al*. Metformin protects against myocardial ischemia-reperfusion injury and cell pyroptosis *via* AMPK/NLRP3 inflammasome pathway. *Aging* 2020;12(23):24270-24287.

40 Peng DD, Fu MY, Wang MN, *et al*. Targeting TGF-β signal transduction for fibrosis and cancer therapy. *Mol Cancer* 2022;21(1):104.

41 Dasgupta B, Seibel W. Compound C/dorsomorphin: its use and misuse as an AMPK inhibitor. *Methods Mol Biol* 2018;1732:195-202.

42 Rao EY, Zhang YW, Li Q, *et al*. AMPK-dependent and independent effects of AICAR and compound C on T-cell responses. *Oncotarget* 2016;7(23):33783-33795.

43 Jeong HJ, Koo S, Kang YH, *et al*. Hepatoprotective effects of paeonol by suppressing hepatic stellate cell activation *via* inhibition of SMAD2/3 and STAT3 pathways. *Food Sci Biotechnol* 2024;33(8):1939-1946.

44 Thabassum Akhtar Iqbal S, Tirupathi Pichiah PB, Raja S, *et al*. Paeonol reverses adriamycin induced cardiac pathological remodeling through Notch1 signaling reactivation in H9c2 cells and adult zebrafish heart. *Chem Res Toxicol* 2020;33(2):312-323.

45 Wang JL, Wu GY, Chu HP, *et al*. Paeonol derivatives and pharmacological activities: a review of recent progress. *Mini Rev Med Chem* 2020;20(6):466-482.

46 Adki KM, Kulkarni YA. Chemistry, pharmacokinetics, pharmacology and recent novel drug delivery systems of paeonol. *Life Sci* 2020;250:117544.